Excitonic Instability in $Ta_2Pd_3Te_5$ Monolayer

Jingyu Yao[1,2†], Haohao Sheng[1,2†], Ruihan Zhang[1,2], Rongtian Pang[3], Jin-Jian Zhou[3*], Quansheng Wu[1,2], Hongming Weng[1,2], Xi Dai[4], Zhong Fang[1,2], and Zhijun Wang[1,2*]

[1]*Beijing National Laboratory for Condensed Matter Physics, and Institute of Physics, Chinese Academy of Sciences, Beijing 100190, China*
[2]*University of Chinese Academy of Sciences, Beijing 100049, China*
[3]*Centre for Quantum Physics, Key Laboratory of Advanced Optoelectronic Quantum Architecture and Measurement (MOE), School of Physics, Beijing Institute of Technology, Beijing 100081, China*
[4]*Department of Physics, Hong Kong University of Science and Technology, Hong Kong 999077, China*

(Received 3 June 2024; accepted manuscript online 25 July 2024)

By systematic theoretical calculations, we reveal an excitonic insulator (EI) in the $Ta_2Pd_3Te_5$ monolayer. The bulk $Ta_2Pd_3Te_5$ is a van der Waals (vdW) layered compound, whereas the vdW layer can be obtained through exfoliation or molecular-beam epitaxy. First-principles calculations show that the monolayer is a nearly zero-gap semiconductor with the modified Becke–Johnson functional. Due to the same symmetry of the band-edge states, the two-dimensional polarization α_{2D} would be finite as the band gap goes to zero, allowing for an EI state in the compound. Using the first-principles many-body perturbation theory, the *GW* plus Bethe–Salpeter equation calculation reveals that the exciton binding energy is larger than the single-particle band gap, indicating the excitonic instability. The computed phonon spectrum suggests that the monolayer is dynamically stable without lattice distortion. Our findings suggest that the $Ta_2Pd_3Te_5$ monolayer is an excitonic insulator without structural distortion.

DOI: 10.1088/0256-307X/41/9/097101

The excitonic insulator (EI) is an exotic ground state of narrow-gap semiconductors and/or semimetals, arising from the spontaneous condensation of electron–hole pairs bound by attractive Coulomb interactions.[1–12] The excitonic instability usually happens as the excitonic binding energy (E_b) is larger than the single-particle band gap (E_g). Due to the Coulomb screening effect,[13] the EI candidates are rare in bulk compounds. In experiments, two kinds of bulk materials are considered as EIs, e.g., 1T-$TiSe_2$[14,15] and Ta_2NiSe_5.[16–18] Due to the existence of the charge density wave transition or structural distortion, the origin of the phase transition in the two EI candidates is still under debate. The plasmon softening around the transition temperature was proposed to serve as the signature of the EI in 1T-$TiSe_2$.[19] However, this result has not been supported by recent momentum-resolved high-resolution electron energy loss spectroscopy studies.[20] There is some compelling evidence for exciton condensation in artificial structures, such as InAs/GaSb quantum wells[3] and $MoSe_2/WSe_2$ bilayers.[21,22] Specifically, the former represents the first complete experimental and theoretical confirmation of topological excitonic insulators in narrow-gap semiconductor systems. However, the experimental confirmation of the EI state in real materials remains unsolved.

On the other hand, lower dimensionality can significantly weaken the screening effect and result in a larger E_b. However, E_b usually shows a strong dependence on E_g, i.e., $E_b \sim E_g/4$ in two-dimensional (2D) materials.[23] To break this dependence, one strategy is to seek dipole-forbidden transitions near the band edges.[24–27] Thus, some 2D materials are theoretically predicted to be EI candidates, such as GaAs,[24] AlSb,[28] AsO,[27] and $Mo_2MC_2F_2$ (M = Ti, Zr, Hf).[29] Interestingly, some quantum spin Hall insulators with large band inversion can result in the same-parity band-edge states. The topological EI can be achieved in such systems.[27,29] However, these 2D EI candidates still need experimental confirmation.

In this work, we demonstrate that $Ta_2Pd_3Te_5$ monolayer shows the excitonic instability by systematic theoretical calculations. First-principles calculations using modified Becke–Johnson functional suggest that the monolayer has a nearly zero band gap and that the band-edge states have the same C_{2z} symmetry eigenvalue. Upon applying the strains, the 2D polarization α_{2D} shows little response to the reduction of E_g. The band gap was obtained by the *GW* calculation with $E_g = 130$ meV. To calculate E_b, we performed the first-principles *GW*-BSE calculations. The obtained $E_b = 633$ meV is larger than the E_g, indicating excitonic instability. The strain-dependent calculations show that the excitonic insulating phase is robust against small strains. Additionally, the tight-binding (TB) model is constructed to analyze the symmetry of the ex-

†These authors contributed equally to this work.
*Corresponding authors. Email: jjzhou@bit.edu.cn; wzj@iphy.ac.cn
© 2024 Chinese Physical Society and IOP Publishing Ltd

citons. Unlike 1T-$TiSe_2$ and Ta_2NiSe_5, no structural instability is found in the phonon spectrum of this material. Our findings suggest that the $Ta_2Pd_3Te_5$ monolayer is an excitonic insulator without structural distortion.

Calculation Methods. First-principles calculations were performed within the framework of density functional theory (DFT) using the projector augmented wave (PAW) method,[30,31] as implemented in the Vienna *ab initio* simulation package (VASP).[32,33] The $20\times4\times1$ k-point sampling grids were used, and the cut-off energy for plane wave expansion was 500 eV. Phonon spectra were obtained with the finite-difference method using a $2\times2\times1$ supercell, as implemented in the Phonopy package.[34] Considering that the Perdew–Burke–Ernzerhof (PBE) exchange correlation functional[35] underestimates the band gap, the band structures were obtained by using the modified Becke–Johnson (MBJ) functional.[36,37] Moreover, to compute the binding energy E_b,[38] first-principles many-body GW-BSE calculations on top of the PBE band structure were performed with the Coulomb cutoff technique in the Yambo package.[39–41] Quasi-particle (QP) corrections in GW calculations are k-point and band dependent. The same k-point grid and 4 Ry cutoff were used to calculate the dielectric function matrix. The kinetic energy cutoff of 70 Ry was used for the evaluation of the exchange part of the self-energy. Achieving convergence of the G_0W_0 band gap involves employing 300 bands along with an extrapolar correction scheme.[42] One valence band (VB) and two conduction bands (CBs) were included to build the BSE Hamiltonian.

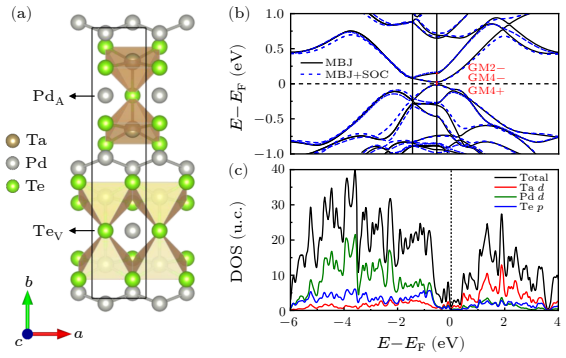

Fig. 1. Crystal structure and band structures of the $Ta_2Pd_3Te_5$ monolayer. (a) Crystal structure of the monolayer. (b) MBJ band structures with and without spin–orbit coupling. The highest VB is labeled by v_1, while the first and second lowest CBs are labeled by c_1 and c_2, respectively. (c) Total and partial DOS for Ta d, Pd d, and Te p orbitals.

Band Structure and Density of States. The van der Waals (vdW) layered compound $Ta_2Pd_3Te_5$ crystallizes in an orthorhombic structure with two vdW layers in a unit cell.[43] The monolayer can be obtained by exfoliation.[43] The two mirror symmetries (M_x, M_y) and inversion symmetry are respected in the monolayer after structural relaxation. Figure 1(a) shows the vdW layer structure with space group $Pmmn$ (No. 59). The quasi-1D chains are along the a (x) direction. The phonon spectrum of the monolayer is obtained in Fig. 2(d). No phonon mode with negative frequency in the phonon spectrum suggests that the monolayer is dynamically stable.

The MBJ band structure along the high-symmetry lines is presented in Fig. 1(b). The irreducible representations (irreps) of the two band-edge states are computed as GM4+ (v_1 band) and GM4− (c_1 band) by the IRVSP program.[44,45] Thus, we define the band gap at Γ by $E_g \equiv E_{GM4-} - E_{GM4+} = 33$ meV, resulting in a nearly zero-gap semiconductor. The spin–orbit coupling (SOC) does not change the band structure at all, but slightly enlarges the band gap to 44 meV. This is because the CBs primarily originate from the Ta-d_{z^2} orbitals with $J_z = 0$, which have little SOC effect. Hereafter, the SOC is neglected in the following calculations. Additionally, the symmetry eigenvalues of the three lowest energy bands are presented in Table 1. They show that the two band-edge bands both have the same C_{2z} symmetry eigenvalue, although they are of different parity. Thus, the 2D polarizability α_{2D} can still be finite when $E_g \to 0$, breaking the strong dependence and allowing for the EI candidate with $E_b > E_g$. Furthermore, due to the significantly enhanced E_b in lower dimensions, the $Ta_2Pd_3Te_5$ layers with the quasi-1D structure present a promising opportunity to realize an intrinsic EI.

Table 1. The symmetry of the highest VB (v_1 band) and the lowest two CBs (c_1 and c_2 bands) at Γ.

Band	Irrep	C_{2z}	M_y
v_1	GM4+	−1	+1
c_1	GM4−	−1	−1
c_2	GM2−	+1	+1

The total and partial densities of states (DOS) are plotted in Fig. 1(c). The results show that the CBs are mainly from Ta d states, while the VBs are mainly from Pd d states. The Te p states have strong hybridization with them, and have certain contributions both below and above the Fermi level (E_F). In particular, the orbital-resolved band structures in Figs. 4(a) and 4(b) show that the CBs are contributed by Ta d_{z^2} states, while the VBs are formed by the hybridization of Pd_A d_{xz} and Te_V p_x states.[46] The related bonds are $d_{Ta-Pd_A} = 2.99$ Å and $d_{Ta-Te_V} = 2.82$ Å, respectively. Although these bond hoppings are allowed, the CB and VB states do not mix on the line $Y\Gamma$ due to their different M_x eigenvalues. The interaction between Ta-d electrons and the Pd-d/Te-p holes may be crucial to the formation of the EI state in the compound.

Evolution of α_{2D} under Strain. As we know, the band gap of this material is sensitive to the strain.[43] Figures 2(a) and 2(b) show the MBJ band structures with uniaxial strains along y. When the system is compressed by 1% in Fig. 2(a), the gap increases to 87 meV; in contrast, it becomes metallic under tensile strain in Fig. 2(b). The 2D polarization, denoted as $\alpha_{2D}^{x/y}$, is calculated with the formula $\alpha_{2D}^{x/y} = c_0\frac{\varepsilon^{xx/yy}-1}{4\pi}$, where c_0 is the thickness of the vacuum in the z direction. The $\varepsilon^{xx/yy}$ represents the xx/yy components of the macroscopic static dielectric ten-

sor, which is computed with the random phase approximation and considering the local field effects, as implemented in VASP.

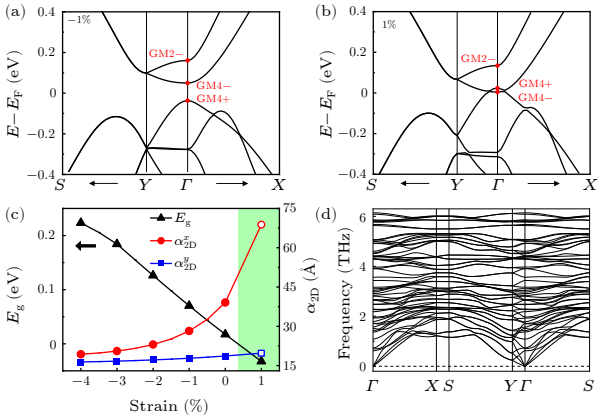

Fig. 2. Evolution of band structures and polarization α_{2D} under uniaxial strain η, $b = (1+\eta)b_0$. [(a), (b)] The band structure with uniaxial strains $\eta = -1\%$ (a) and $+1\%$ (b), respectively. (c) E_g and α_{2D} under different uniaxial strains. (d) The phonon spectrum of $Ta_2Pd_3Te_5$ monolayer. There is no imaginary frequency phonon mode.

In Fig. 2(c), we plot E_g and 2D polarization $\alpha_{2D}^{x/y}$ as a function of the uniaxial strain. In the positive gap range, both of them show a weak dependence on the reduction of the band gap. Especially, α_{2D}^{y} is almost unchanged. The weak dependence of α_{2D}^{x} is attributed to the transition between the v_1 band and the second lowest CB (c_2 band). The symmetry eigenvalues at Γ yield $\langle c_2|\nabla_{k_y}|v_1\rangle = 0$ and $\langle c_2|\nabla_{k_x}|v_1\rangle \neq 0$, which have been confirmed numerically.[47] As aforementioned, the band-edge transition between c_1 and v_1 bands is forbidden due to the twofold rotation. This indicates the decoupling between E_g and E_b in this material with band-edge states of the same C_{2z} symmetry.

Stable Phonon Spectrum. In previous studies,[48,49] the phonon spectra of previous EI candidates 1T-$TiSe_2$ and Ta_2NiSe_5 show the structural instability with imaginary frequency phonon modes. Whether the charge-density-wave transition in 1T-$TiSe_2$ comes from the Jahn–Teller mechanism or from the excitonic instability has plagued the EI community for decades. Additionally, as indicated by the imaginary frequency mode, the structure distortion of Ta_2NiSe_5 from *Cmcm* (SG No. 63) to *C*2/*c* (SG No. 15) occurs at 328 K,[50–52] accompanied by a metal-to-insulator transition even in the single-particle band structure calculations.

However, our calculation shows that there is no imaginary frequency on the phonon spectrum of $Ta_2Pd_3Te_5$ monolayer in Fig. 2(d). Even if we start from some degree of distortion, the relaxation still yields the *Pmmn* symmetry structure. The phonon spectrum of the bulk $Ta_2Pd_3Te_5$ also does not show any imaginary frequency modes, quite different from the previous two examples. Experimentally, no structural distortion is found in the x-ray diffraction data.[43] Therefore, $Ta_2Pd_3Te_5$ inherently excludes Jahn–Teller-like instabilities, consequently avoiding the confusion of 1T-$TiSe_2$ or Ta_2NiSe_5. However, the lack of a structural signal usually poses challenges for identifying an EI phase transition. The symmetry breaking of the EI phase transition could be weakly coupled to the lattice structure, which needs high-resolution measurements, such as electron diffraction.

Binding Energy and GW-BSE Calculations. In order to investigate the excitonic instability, we carry out many-body *GW* calculations in a one-shot scheme (G_0W_0). The *GW* band structure in Fig. 3(a) does not change significantly from the MBJ one except that the E_g changes from 33 meV to 130 meV. The first-principles *GW*-BSE calculation shows that $E_b = 633$ meV. This E_b value exceeds the *GW* band gap E_g. The lowest-energy exciton wavefunction in real space is shown in Fig. 3(c) as the conditional probability of finding a bound electron (red), provided that the hole position is fixed (black dot). The electron is well-localized around the hole, within a radius of 30 Å. The lowest-energy exciton probability weight in momentum space is localized around the Γ point, as shown in Fig. 3(d).

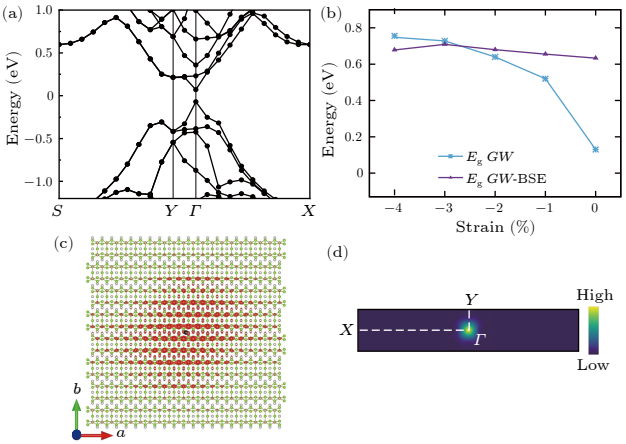

Fig. 3. (a) The G_0W_0 band structure. (b) Strain dependence of E_g and E_b. The results show an intrinsic EI with $E_b > E_g$ at $\eta > -2\%$. (c) Exciton wavefunction square modulus, as obtained from the Bethe–Salpeter equation (*GW*-BSE). The contour plot (red) is the probability density of locating the bound electron once the hole position is fixed (black dot). The figure contains 20 and 4 unit cells in the x and y directions, respectively. We note that it is well-localized around the hole. (d) Exciton wavefunction square modulus in reciprocal space. The exciton probability weight is localized around Γ point.

In order to study the strain dependence of E_b, we performed the one-shot *GW*-BSE calculations under uniaxial compressive strains. Figure 3(b) shows E_b as a function of compressive strains. The obtained E_b exceeds the E_g at $\eta > -2\%$, indicating that the EI instability is robust against small strains in the $Ta_2Pd_3Te_5$ monolayer. We observe that the obtained E_b is almost unchanged, although E_g varies with different strains. We attribute this to the unique wavefunctions of the conduction and valence states, which originate from Ta and Pd/Te atoms, respectively (Fig. 4). The E_b in the $Ta_2Pd_3Te_5$ monolayer shows little response to the change of E_g under strain, as illustrated in

Fig. 3(b). Although the exact E_g is difficult to predict and the strain condition varies in experiment, the formation of EI is accessible at modest experimental conditions.

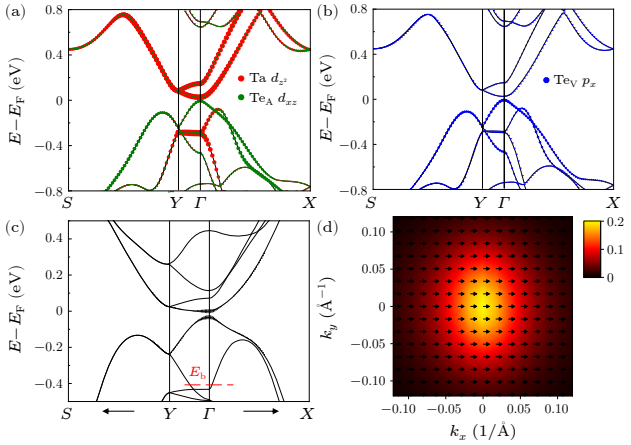

Fig. 4. [(a), (b)] The orbital-resolved MBJ band structures for Ta d_{z^2}, Pd_A d_{xz}, and Te_V p_x orbitals. (c) The band structure of the effective TB model. The band spread corresponds to the contribution of a particular electron–hole transition to the lowest-energy exciton. (d) Absolute values (color) and phase angles (arrows) of the lowest-energy exciton wavefunction.

Tight-Binding Model and Symmetry Analysis. In order to analyze the symmetry of the excitons, we construct a TB model and perform TB-BSE calculations to obtain the phases of the exciton wavefunctions. In the orbital-resolved band structures presented in Figs. 4(a) and 4(b), we find that the valence bands are mainly formed by the Pd_A d_{xz} states, which hybridize with the Te p_x states (especially Te_V). The CBs are from the Ta d_{z^2} states, which do not hybridize with the valence bands along Y–Γ line. Accordingly, we construct a sixteen-band Wannier-based TB Hamiltonian, extracted from the DFT calculations by using Wannier90 package.[53] Under the basis of these Wannier orbitals $\{|\alpha\boldsymbol{k}\rangle\}$, the eigenvalues and eigenstates of $H_{\rm TB}$ yield $\hat{H}_{\rm TB}(\boldsymbol{k})|b\boldsymbol{k}\rangle = E_b(\boldsymbol{k})|b\boldsymbol{k}\rangle$. On top of the TB model in Fig. 4(c), we have solved the model BSE to find the collective modes. The BSE reads[54–56]

$$(\Omega_S - E_c(\boldsymbol{k}) + E_v(\boldsymbol{k}))A^S_{cv}(\boldsymbol{k}) = \sum_{c'v'\boldsymbol{k}'} \mathcal{K}^{cv\boldsymbol{k}}_{c'v'\boldsymbol{k}'} A^S_{c'v'}(\boldsymbol{k}'), \quad (1)$$

where c and v are the labels of conduction and valence bands, Ω_S is the energy of exciton eigenstates, $|S\rangle \equiv \sum_{cv\boldsymbol{k}} A^S_{cv}(\boldsymbol{k})\hat{c}^\dagger_{c\boldsymbol{k}}\hat{c}_{v\boldsymbol{k}}|0\rangle$, and $|0\rangle$ is the non-interacting ground state. The kernel consists of the direct part $\mathcal{K}^d$ and the exchange part $\mathcal{K}^x$,

$$\begin{aligned}
\mathcal{K}^{cv\boldsymbol{k}}_{c'v'\boldsymbol{k}'} &= \mathcal{K}^{dcv\boldsymbol{k}}_{c'v'\boldsymbol{k}'} + \mathcal{K}^{xcv\boldsymbol{k}}_{c'v'\boldsymbol{k}'},\\
\mathcal{K}^{xcv\boldsymbol{k}}_{c'v'\boldsymbol{k}'} &= -V f_{cv}(\boldsymbol{k},\boldsymbol{k}) f_{v'c'}(\boldsymbol{k}',\boldsymbol{k}'),\\
\mathcal{K}^{dcv\boldsymbol{k}}_{c'v'\boldsymbol{k}'} &= -W(\boldsymbol{k}-\boldsymbol{k}') f_{cc'}(\boldsymbol{k},\boldsymbol{k}') f_{v'v}(\boldsymbol{k}',\boldsymbol{k}). \quad (2)
\end{aligned}$$

Here V is the bare Coulomb potential, and $W(\boldsymbol{q}) = 2\pi e^2/[S|\boldsymbol{q}|(1+\alpha_{2D}|\boldsymbol{q}|)]$ is the screened Coulomb potential,[57,58] where S is the system area and the computed 2D polarization $\alpha_{2D} = 17.854$ Å is used. We define $f_{b_1b_2}(\boldsymbol{k},\boldsymbol{k}') \equiv \sum_\alpha \langle b_1\boldsymbol{k}|\alpha\boldsymbol{k}\rangle\langle\alpha\boldsymbol{k}'|b_2\boldsymbol{k}'\rangle$, $b_1, b_2 \in \{c, v\}$. Since $f_{cv}(\boldsymbol{k},\boldsymbol{k}) = 0$, $\mathcal{K}^x_{cv\boldsymbol{k},\,c'v'\boldsymbol{k}'} = 0$. By solving Eq. (1), one can obtain the discrete excitonic binding energies with electron–hole attractive Coulomb interactions. The lowest excitonic binding energy is depicted in Fig. 4(c), which is larger than the band gap, indicating the excitonic phase. This exciton wavefunction is given in Fig. 4(d), where colors and arrows indicate the distribution of absolute values and phase angles, respectively. It is 1s-like in the vicinity of the Γ point, which is consistent with the DFT result in Fig. 3(d). As the band-edge states belong to GM4+ and GM4− irreps, respectively, the 1s-like excitonic state breaks spatial inversion and all mirror symmetries.

Discussion. In this work, we demonstrate that the $Ta_2Pd_3Te_5$ monolayer is an excitonic insulator by first-principles GW-BSE calculations. In the single-particle picture, the MBJ calculation shows that the monolayer is a nearly zero-gap semiconductor. The low-energy states at Γ have the same C_{2z} symmetry eigenvalue, making the band-edge transitions forbidden and keeping the α_{2D} finite as $E_g \to 0$. By applying the uniaxial strains, the α_{2D} shows little response to the reduction of E_g as is expected. The G_0W_0 band gap $E_g = 130$ meV and $E_b = 633$ meV is obtained by performing one-shot GW-BSE calculations in Yambo, indicating an intrinsic EI with $E_b > E_g$. By investigating the strain effect, we find that the strong excitonic instability is robust against small strains, and the E_b shows little response to the change of E_g. Although the E_b may be slightly modified in the self-consistent GW-BSE calculations, the EI phase would form as the gap goes to zero under strain. Therefore, we conclude that the excitonic insulator phase in the $Ta_2Pd_3Te_5$ monolayer is achievable in experiments.

In the vdW layered $Ta_2Pd_3Te_5$ bulk, the band-edge states at Γ have the same parity in the bulk MBJ band structure, making transitions between them forbidden. The decoupled relationship between E_g and E_b remains, making the EI phase possible in the bulk crystals. In addition, the layered compound possesses several advantages. To begin with, in the series of the $A_2M_3X_5$ (A = Ta, Nb; M = Pd, Ni; X = Se, Te) family, the band gap is modified by chemical doping. Unlike the small gap semiconductor $Ta_2Ni_3Te_5$ with higher-order topology[46] and the metallic compound $Nb_2Pd_3Te_5$ with superconductivity,[59] the $Ta_2Pd_3Te_5$ is a nearly zero-gap semiconductor, exhibiting strong EI instability. Furthermore, it is a vdW layered compound with 1D chains and strong anisotropy, where the screening effect is relatively weak, resulting in a large excitonic binding energy. Moreover, the chemical potential of the crystals is right in the tiny band gap in experiments, showing the ideal balance of electrons and holes for excitonic condensation. Finally, the layered compound is easy to exfoliate and to fabricate into devices, and its properties can be readily tuned by gate voltage. Therefore, we conjecture that the EI state is also promising in the few-layer flakes and bulk samples.

Note Added. In the preparation of this work, two collaborative experimental studies have been conducted on the bulk crystals.[60,61] In the finalizing stage, we noticed

another related experimental work.[62]

Acknowledgements. We thank Xinzheng Li, Huaiyuan Yang, and Yuelin Shao for helpful discussions. This work was supported by the National Natural Science Foundation of China (Grant Nos. 11974395 and 12188101), the Strategic Priority Research Program of Chinese Academy of Sciences (Grant No. XDB33000000), the National Key R&D Program of China (Grant Nos. 2022YFA1403800 and 2022YFA1403400), and the Center for Materials Genome.

References

[1] Jérome D, Rice T M, and Kohn W 1967 *Phys. Rev.* **158** 462
[2] Shim Y P and MacDonald A H 2009 *Phys. Rev. B* **79** 235329
[3] Du L, Li X, Lou W, Sullivan G, Chang K, Kono J, and Du R R 2017 *Nat. Commun.* **8** 1971
[4] Sun B, Zhao W, Palomaki T, Fei Z, Runburg E, Malinowski P, Huang X, Cenker J, Cui Y T, Chu J H, Xu X, Ataei S S, Varsano D, Palummo M, Molinari E, Rontani M, and Cobden D H 2022 *Nat. Phys.* **18** 94
[5] Jia Y, Wang P, Chiu C L, Song Z, Yu G, Jäck B, Lei S, Klemenz S, Cevallos F A, Onyszczak M, Fishchenko N, Liu X, Farahi G, Xie F, Xu Y, Watanabe K, Taniguchi T, Bernevig B A, Cava R J, Schoop L M, Yazdani A, and Wu S 2022 *Nat. Phys.* **18** 87
[6] Kong L, Shindou R, and Zhang Y 2022 *Phys. Rev. B* **106** 235145
[7] Gao Q, Chan Y H, Wang Y, Zhang H, Jinxu P, Cui S, Yang Y, Liu Z, Shen D, Sun Z, Jiang J, Chiang T C, and Chen P 2023 *Nat. Commun.* **14** 994
[8] Song Y, Jia C, Xiong H, Wang B, Jiang Z, Huang K, Hwang J, Li Z, Hwang C, Liu Z, Shen D, Sobota J A, Kirchmann P, Xue J, Devereaux T P, Mo S K, Shen Z X, and Tang S 2023 *Nat. Commun.* **14** 1116
[9] Wang R, Sedrakyan T A, Wang B, Du L, and Du R R 2023 *Nature* **619** 57
[10] Pikulin D I and Hyart T 2014 *Phys. Rev. Lett.* **112** 176403
[11] Ma J, Nie S, Gui X, Naamneh M, Jandke J, Xi C, Zhang J, Shang T, Xiong Y, Kapon I, Kumar N, Soh Y, Gosálbez-Martínez D, Yazyev O V, Fan W, Hübener H, Giovannini U D, Plumb N C, Radovic M, Sentef M A, Xie W, Wang Z, Mudry C, Müller M, and Shi M 2022 *Nat. Mater.* **21** 423
[12] Shao Y and Dai X 2023 2024 *Phys. Rev. X* **14** 021047
[13] Rohlfing M, Krüger P, and Pollmann J 1993 *Phys. Rev. B* **48** 17791
[14] Cercellier H, Monney C, Clerc F, Battaglia C, Despont L, Garnier M G, Beck H, Aebi P, Patthey L, Berger H, and Forró L 2007 *Phys. Rev. Lett.* **99** 146403
[15] Monney C, Cercellier H, Clerc F, Battaglia C, Schwier E F, Didiot C, Garnier M G, Beck H, Aebi P, Berger H, Forró L, and Patthey L 2009 *Phys. Rev. B* **79** 045116
[16] Wakisaka Y, Sudayama T, Takubo K, Mizokawa T, Arita M, Namatame H, Taniguchi M, Katayama N, Nohara M, and Takagi H 2009 *Phys. Rev. Lett.* **103** 026402
[17] Wakisaka Y, Sudayama T, Takubo K, Mizokawa T, Saini N L, Arita M, Namatame H, Taniguchi M, Katayama N, Nohara M, and Takagi H 2012 *J. Superconduct. Novel Magn.* **25** 1231
[18] Mazza G, Rösner M, Windgätter L, Latini S, Hübener H, Millis A J, Rubio A, and Georges A 2020 *Phys. Rev. Lett.* **124** 197601
[19] Kogar A, Rak M S, Vig S, Husain A A, Flicker F, Joe Y I, Venema L, MacDougall G J, Chiang T C, Fradkin E, van Wezel J, and Abbamonte P 2017 *Science* **358** 1314
[20] Lin Z, Wang C, Balassis A, Echeverry J P, Vasenko A S, Silkin V M, Chulkov E V, Shi Y, Zhang J, Guo J, and Zhu X 2022 *Phys. Rev. Lett.* **129** 187601
[21] Wang Z, Rhodes D A, Watanabe K, Taniguchi T, Hone J C, Shan J, and Mak K F 2019 *Nature* **574** 76
[22] Troue M, Figueiredo J, Sigl L, Paspalides C, Katzer M, Taniguchi T, Watanabe K, Selig M, Knorr A, Wurstbauer U, and Holleitner A W 2023 *Phys. Rev. Lett.* **131** 036902
[23] Jiang Z, Liu Z, Li Y, and Duan W 2017 *Phys. Rev. Lett.* **118** 266401
[24] Jiang Z, Li Y, Zhang S, and Duan W 2018 *Phys. Rev. B* **98** 081408
[25] Jiang Z, Li Y, Duan W, and Zhang S 2019 *Phys. Rev. Lett.* **122** 236402
[26] Jiang Z, Lou W, Liu Y, Li Y, Song H, Chang K, Duan W, and Zhang S 2020 *Phys. Rev. Lett.* **124** 166401
[27] Yang H, Zeng J, Shao Y, Xu Y, Dai X, and Li X Z 2024 *Phys. Rev. B* **109** 075167
[28] Dong S and Li Y 2021 *Phys. Rev. B* **104** 085133
[29] Dong S and Li Y 2023 *Phys. Rev. B* **107** 235147
[30] Blöchl P E 1994 *Phys. Rev. B* **50** 17953
[31] Kresse G and Joubert D 1999 *Phys. Rev. B* **59** 1758
[32] Kresse G and Furthmüller J 1996 *Comput. Mater. Sci.* **6** 15
[33] Kresse G and Furthmüller J 1996 *Phys. Rev. B* **54** 11169
[34] Togo A and Tanaka I 2015 *Scr. Mater.* **108** 1
[35] Perdew J P, Burke K, and Ernzerhof M 1996 *Phys. Rev. Lett.* **77** 3865
[36] Tran F and Blaha P 2009 *Phys. Rev. Lett.* **102** 226401
[37] Becke A D and Johnson E R 2006 *J. Chem. Phys.* **124** 221101
[38] Yamada T and Hirata S 2015 *J. Chem. Phys.* **143** 114112
[39] Marini A, Hogan C, Grüning M, and Varsano D 2009 *Comput. Phys. Commun.* **180** 1392
[40] Giannozzi P, Baroni S, Bonini N, Calandra M, Car R, Cavazzoni C, Ceresoli D, Chiarotti G L, Cococcioni M, Dabo I, Dal Corso A, de Gironcoli S, Fabris S, Fratesi G, Gebauer R, Gerstmann U, Gougoussis C, Kokalj A, Lazzeri M, Martin-Samos L, Marzari N, Mauri F, Mazzarello R, Paolini S, Pasquarello A, Paulatto L, Sbraccia C, Scandolo S, Sclauzero G, Seitsonen A P, Smogunov A, Umari P, and Wentzcovitch R M 2009 *J. Phys.: Condens. Matter* **21** 395502
[41] Rozzi C A, Varsano D, Marini A, Gross E K U, and Rubio A 2006 *Phys. Rev. B* **73** 205119
[42] Bruneval F and Gonze X 2008 *Phys. Rev. B* **78** 085125
[43] Guo Z, Yan D, Sheng H, Nie S, Shi Y, and Wang Z 2021 *Phys. Rev. B* **103** 115145
[44] Gao J, Wu Q, Persson C, and Wang Z 2021 *Comput. Phys. Commun.* **261** 107760
[45] Zhang R, Deng J, Sun Y, Fang Z, Guo Z, and Wang Z 2023 *Phys. Rev. Res.* **5** 023142
[46] Guo Z, Deng J, Xie Y, and Wang Z 2022 *npj Quantum Mater.* **7** 87
[47] Zhang S, Sheng H, Song Z D, Liang C, Jiang Y, Sun S, Wu Q, Weng H, Fang Z, Dai X, and Wang Z 2023 *Chin. Phys. Lett.* **40** 127101
[48] Calandra M and Mauri F 2011 *Phys. Rev. Lett.* **106** 196406
[49] Bianco R, Calandra M, and Mauri F 2015 *Phys. Rev. B* **92** 094107
[50] Di Salvo F J, Chen C H, Fleming R M, Waszczak J V, Dunn R G, Sunshine S A, and Ibers J A 1986 *J. Less Common Met.* **116** 51

[51] Nakano A, Hasegawa T, Tamura S, Katayama N, Tsutsui S, and Sawa H 2018 *Phys. Rev. B* **98** 045139
[52] Kim S Y, Kim Y, Kang C J, An E S, Kim H K, Eom M J, Lee M, Park C, Kim T H, Choi H C, Min B I, and Kim J S 2016 *ACS Nano* **10** 8888
[53] Pizzi G, Vitale V, Arita R, Blügel S, Freimuth F, Géranton G, Gibertini M, Gresch D, Johnson C, Koretsune T, Ibañez-Azpiroz J, Lee H, Lihm J M, Marchand D, Marrazzo A, Mokrousov Y, Mustafa J I, Nohara Y, Nomura Y, Paulatto L, Poncé S, Ponweiser T, Qiao J, Thöle F, Tsirkin S S, Wierzbowska M, Marzari N, Vanderbilt D, Souza I, Mostofi A A, and Yates J R 2020 *J. Phys.: Condens. Matter* **32** 165902
[54] Rohlfing M and Louie S G 2000 *Phys. Rev. B* **62** 4927
[55] Scharf B, Xu G, Matos-Abiague A, and Žutić I 2017 *Phys. Rev. Lett.* **119** 127403
[56] Quintela M F C M, Henriques J C G, Tenório L G M, and Peres N M R 2022 *Phys. Status Solidi* **259** 2200097
[57] Cudazzo P, Tokatly I V, and Rubio A 2011 *Phys. Rev. B* **84** 085406
[58] Yang H, Wang X, and Li X Z 2022 *New J. Phys.* **24** 083010
[59] Higashihara N, Okamoto Y, Yoshikawa Y, Yamakawa Y, Takatsu H, Kageyama H, and Takenaka K 2021 *J. Phys. Soc. Jpn.* **90** 063705
[60] Huang J, Jiang B, Yao J, Yan D, Lei X, Gao J, Guo Z, Jin F, Li Y, Yuan Z, Chai C, Sheng H, Pan M, Chen F, Liu J, Gao S, Qu G, Liu B, Jiang Z, Liu Z, Ma X, Zhou S, Huang Y, Yun C, Zhang Q, Li S, Jin S, Ding H, Shen J, Su D, Shi Y, Wang Z, and Qian T 2024 *Phys. Rev. X* **14** 011046
[61] Zhang P, Dong Y Y, Yan D Y, Jiang B, Yang T, Li J, Guo Z P, Huang Y, Haobo Q, Li Y P, Li K, Kurokawa R, Wang Y F, Nie M, Hashimoto D, Lu W H, Jiao J, Shen T, Qian Z J, Wang Y G, Shi T, and Kondo T 2024 *Phys. Rev. X* **14** 011047
[62] Hossain M S, Cochran T A, Jiang Y X, Zhang S B, Wu H Y, Liu X X, Zheng X Q, Kim B, Cheng G M, Zhang Q, Litskevich M, Zhang J Y, Cheng Z J, Liu J J, Yin J X, Yang X P, Denlinger J, Tallarida M, Dai J, Vescovo E, Rajapitamahuni A, Miao H, Yao N, Peng Y Y, Yao Y G, Wang Z W, Balicas L, Neupert T, and Hasan M Z 2023 arXiv:2312.15862 [cond-mat.str-el]